Journal of Advanced Ceramics
2017, **6**(2): 157–164
DOI: 10.1007/s40145-017-0228-2

ISSN 2226-4108
CN 10-1154/TQ

Research Article

Controlling calcium and phosphate ion release of 3D printed bioactive ceramic scaffolds: An *in vitro* study

Lukasz WITEK[a,*], Yang SHI[b], James SMAY[c]

[a]*Department of Biomaterials and Biomimetics*, *College of Dentistry*, *New York University*, *New York*, *NY*, *USA*
[b]*School of Chemical Engineering*, *Oklahoma State University*, *Stillwater*, *OK*, *USA*
[c]*School of Materials Science and Engineering*, *Oklahoma State University*, *Tulsa*, *OK*, *USA*

Received: December 28, 2016; Revised: March 26, 2017; Accepted: April 13, 2017
© The Author(s) 2017. This article is published with open access at Springerlink.com

Abstract: This paper characterizes in an *in vitro* setting the release of calcium (Ca) and phosphate (PO_4) of 3D printed bioactive ceramic scaffold prepared from extrudable paste containing hydroxyapatite and β-tricalcium phosphate (β-TCP). Hydroxyapatite and β-TCP were calcined at 800 ℃ for 11 h, fabricated into four experimental groups (100% HA, 100% β-TCP, 15%/85% HA/β-TCP, and 15%/85% HA/β-TCP (design)), sintered to 1100 ℃ for 4 h. Calcium and phosphorus concentrations were evaluated using ICP spectroscopy, and the release of Ca and PO_4 ions during dissolution of the CaP-based scaffolds was measured by submerging in 0.05 mol/L Tris(hydroxymethyl)aminomethane-HCl and maintaining a temperature of 37 ℃. The Ca and PO_4 concentrations of the solutions were measured with the utilization of a calcium assay kit and a phosphate assay kit and read in a UV–visible spectrophotometer. The 100% HA scaffold group showed the greatest concentration of Ca ions (~1.9 mg/dL), but ultimately released at a lower amount as time increased; the 100% HA scaffold also showed the lowest total amount of calcium ions released over the course of evaluation. The results for the 100% β-TCP were on the opposite of the HA with the highest amount of calcium ion release over the study. While the PO_4 ion release showed a similar trend as those observed with Ca ions with an apparent difference in the 100% HA scaffold group. There was nearly 0 mg/dL of the phosphate ions released in the first 24 h, in comparison to the amount of Ca ions released during the same time frame. Since various formulations can lead to different properties of these bioactive ceramic scaffolds, it is important to understand how the tailoring of this important biphasic material can impact the long-term outcome of an ever-important *in vivo* clinical trial in the future.

Keywords: 3D printing; β-TCP; scaffolds; *in vitro*; calcium; phoshpate

1 Introduction

Bone wound healing is a complicated area of research, which has doctors, engineers, and scientists continuously searching for the most appropriate solutions. Currently there are no “ideal” options on the market to repair large, critical sized defects or load bearing areas. The future of bone grafting is leading towards the combination of materials and fabrication

* Corresponding author.
E-mail: lukasz.witek@nyu.edu

processes, which will allow for fabrication of "tailor-able" devices.

The repair of critical sized long bone defects is of special interest in the orthopedic field due to its reconstructive complexity. Much attention has been given to the defect site's blood supply, with focus between bone and immune cells and mechanical reestablishment. Most commonly, the defects are caused by birth defect, trauma, or tumor resection. These issues may leave the patient with a critical sized defect, which must be controlled with suitable dead space management followed by bone reconstruction utilizing a grafting material or device, which is osteoconductive and degradable, while simultaneously minimizing complications and shortening the duration of recovery.

Currently, the viable bone grafting material solution is calcium phosphate (CaP)-based, which possesses two (*osteoconduction* and *osseointegration*) of the following three properties: *osteoconduction*—the capability to support the growth of bone over its surface; *osteogenesis*—the process of extra cellular matrix deposition and subsequent mineralization by osteoblasts; and *osseointegration*—the ability to intimately interact with bone without an extra layer of soft tissue. However, different host-to-grafting material responses have been reported and should be taken into consideration while determining treatment options.

The stability of calcium phosphate-based ceramics is known to be compositionally and structurally dependent [1], depending on the materials hydroxyapatite (HA), beta tri-calcium phosphate (β-TCP), or biphasic calcium phosphate (BCP). When these CaP-composed devices are implanted, the ceramic will undergo dissolution at different rates (HA < β-TCP < α-TCP) [2,3]. Additionally, when placed *in vivo*, the CaP ceramics induce a precipitation of a phase which is comparable to the HA-like mineral found in bone [4]. While in some instances it has been seen that a bone apatite-like material was formed in nonosseous sites [3,4]. Therefore, an important factor with regards to bioactivity (bone tissue formation rate and bone tissue bonding) is the release of ions from the dissolution of CaP ceramics, which in turn may affect cellular activity, organic matrix deposition, or mineral deposition [5,6].

There was an analysis and assessment of the dissolution of 3D printed lattice-based bioactive ceramic scaffolds (LBBCS) [7]. In an *in vitro* setting, it is of value to qualitatively and quantitatively analyze and observe any possible phase changes, which can possibly occur during the fabrication process or dissolution process [8,9]. In the past, there has been work done to try to interpret as well as predict the long-term effects of the dissolution of CaP ceramics. This study is set out to determine the relative dissolution behavior of four experimental groups (Table 1) specifically the mean concentrations (mg/dL) of Ca and PO_4 ions which were released from the 3D printed grafting devices in a Tris(hydroxymethyl) aminomethane-HCl buffer environment [4].

2 Materials and methods

2. 1 Ink preparation

Prior to 3D printing, the formulated colloidal gel was subjected to a series of powder processing steps at the beginning (e.g., calcining, attrition milling, and drying of the individual base materials), which is described in detail by Witek *et al.* [7]. The aforementioned processed ceramic powders were utilized for the colloidal ink suspension, with a solid volume fraction (φ_{solid}) of approximately 46% ceramics, (i.e., 100% HA (0.7 μm in particle size), 100% β-TCP (0.4 μm in particle size), or pre-determined ratio of HA:β-TCP) [10]. Upon calculating the appropriate amounts of ceramic powders, H_2O, and dispersant, Darvan®821A (R.T. Vanderbilt Company, Inc., Norwalk, CT, USA), ~15 mg/g of ceramic, the materials were added to a mixing container in which the bottom was charged with zirconia milling media (5 mm; Union Process, Akron, OH, USA). The mixture was spun in a conditioning mixer (THINKY AR-250; Thinky, Tokyo, Japan) for 180 s at 2000 rpm. The next step was the addition of a thickening agent, Methylcellulose F4M (Dow Chemical Company, Midland, MI, USA), approximately 8 mg/mL of ceramic, followed by spinning for ~120 s at 2000 rpm. The final step was the addition of a gelling mechanism (polyethlyenimine (PEI); Sigma-Aldrich St. Louis, MO, USA). About 200 mg of polyethyleneimine per 30 mL of ink was added followed by spinning to achieve the desired consistency.

After the colloidal gel was prepared, it was 3D printed into circular lattice scaffolds (Fig. 1).

Table 1 Summary of the four primary experimental scaffold groups used for the *in vitro* dissolution evaluation of Ca and PO_4 release over a set amount of time

Group	Description	Abbreviation
1	100% HA	HA
2	100% β-TCP	β-TCP
3	15%/85% HA/β-TCP	BCP
4	15%/85% HA/β-TCP(design)	BCP (design)

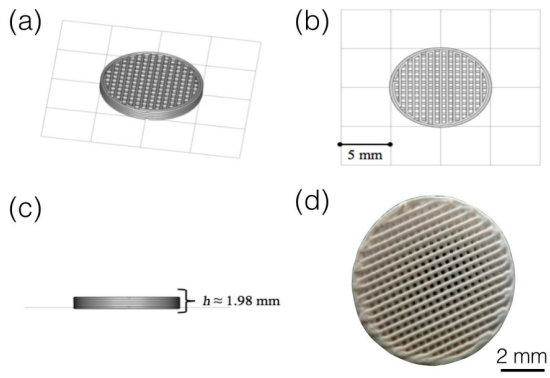

Fig. 1 Schematic of scaffold designed in RoboCAD 4.3 (3D Inks, LLC Tulsa, OK, USA): (a) isometric view, (b) top view, (c) front/side view, and (d) final scaffold after sintering.

2. 2 Sample fabrication

The 3D direct-writing printer used a gantry robot with affixed syringe pumps to extrude the colloidal inks through a fine nozzle to build the 3D scaffold [11,12]. The 3D disc-shaped scaffolds (10 mm in diameter, ~2 mm in thickness, 330 μm in struts, and 500 μm in pore size) were designed on a computer-aided design (CAD) software (RoboCAD 4.3, 3D Inks, LLC Tulsa, OK, USA) (Fig. 1). The 3D disc-shaped scaffolds were printed layer-by-layer at 10 mm/s deposition rate onto a flat ceramic substrate (ADS-96R, Coors Tek, Grand Junction, CO, USA) in low-viscosity paraffin oil (Ultra-Pure lamp oil, Lamplight Farms Inc., Menomonee Falls, WI, USA) to prevent drying of the structure during assembly.

After the scaffolds were fabricated, they were removed from the oil bath and allowed to dry in air for ~12 h prior to the sintering process. Heat treatment of the scaffolds was performed utilizing an electric furnace (Model LHT 02/17, Nabertherm GmbH, Lilienthal, Germany) to enhance the mechanical strength for handling during the experiments (e.g., *in vitro* dissolution study) [11]. During the sintering processing, the green body ceramics were densified and organic components were burned off. The firing protocol began by heating at 2 ℃/min until 400 ℃, dwelling at 400 ℃ for 2 h, then heating until 900 ℃ (~8 ℃/min), dwelling for 2 h at 900 ℃, heating at 3.3 ℃/min to ultimate temperature of 1100 ℃, dwelling at 1100 ℃ for 4 h, and finally cooling at ~8.0 ℃/min until the samples were cooled to room temperature (~30 ℃). The binder burnout during the sintering process resulted in a predictable volumetric shrinkage (~20%) and defects such as cracking and warping [10]. The sintering shrinkage of ceramics is an unavoidable step, and all dimensions of the designed geometric structure must be enlarged to account for this phenomena and to ultimately attain the final desired dimensions.

2. 3 Chemical characterization

Calcium (Ca) and phosphorus (P) concentrations were evaluated using inductively coupled plasma (ICP) spectroscopy (Thermo Jarell Ash, Trace Advantage, Franklin, MA, USA). For this objective, 10 mg of powders from each experimental group were dissolved in 35% HCl solution and mixed 100 mL of double distilled water in a volumetric flask. Suitable standard solutions for Ca (0, 20, and 40 ppm) and P (0, 10, and 40 ppm) were prepared from 100 ppm standard solutions of the respective elements (Fisher Scientific, Pittsburgh, PA, USA). Each specimen in solution and standard solution was pumped through argon plasma, which was excited by a 2 kW, 27.12 MHz radio frequency generator [13]. Additionally scaffold groups were subjected to energy-dispersive X-ray spectroscopy (Hitachi S-4800, Schaumburg, IL, USA) for further verification of their respective Ca:P ratios.

X-ray diffraction (XRD; Bruker AXS D8 Discover, Madison, WI, USA) was used to determine the crystalline phases present within the raw materials and experimental groups. Three different spectra from each testing group were obtained ($n = 3$ per group). The diffractometer was operated by using a curved crystal monochromator, operating at 45 mA and 45 kV, and scanned in 2θ range from 20° to 65° [7], with a step size of 0.02° at 3 s/step.

Rietveld refinement analysis used the data collected from X-ray diffraction, and subsequently converted data to "*.xy*" format. The raw data was then input into Material Analysis Using Diffraction (MAUD) software for quantitative analysis. Rietveld analysis utilized the samples from previous XRD spectra (i.e., peak, height, width, and position). This refinement method was used to quantify the percentage of each phase (HA, β-TCP, and other commonly observed phases in calcium- and phosphate-based materials such as calcium oxide, CaO) present in different calcination temperatures and sintering groups. A least-squares fit approach was utilized to measured scans until replicating a theoretical scan (based on the structure in Inorganic Crystal Structure Data Base (ICSD)) [14,15]. The background, cell parameters, preferred orientation, peak asymmetry, atomic positions, site occupancy factors, and global

vibrational parameters were refined.

The *in vitro* observation for the release of Ca and PO_4 ions during dissolution of the CaP-based scaffolds, was measured by submerging LBBCS in a 24 well plate (Corning® Costar®, Sigma-Aldrich, St. Louis, MO, USA) ($n = 1$ scaffold/well) containing 0.05 mol/L Tris(hydroxymethyl)aminomethane-HCl (bioWORLD, Dublin, OH, USA) solution with a pH of ~7.3 and maintaining a temperature of 37 ℃ (in an incubator). The weight of scaffold to volume of solution ratio was ~1 mg/mL as recommended by Ducheyne *et al.* [4]. The time periods to be examined for the release of ions was from 1 h ranging to 2 weeks, with samples measured in triplicate for each time point. The Ca and PO_4 concentrations of the solutions were measured with the utilization of a calcium assay kit (QuantiChrom™ Calcium Assay Kit (DICA-500), BioAssay Systems, Hayward, CA, USA) and a phosphate assay kit (Malachite Green Phosphate Assay Kit (POMG-25H), BioAssay Systems, Hayward, CA, USA), read in a UV–visible spectrophotometer (Cary 5000 UV-Vis-NIR, Santa Clara, CA, USA).

2. 4 Statistical analysis

For statistical evaluation, analysis of variance (ANOVA) at a 95% confidence interval by using IBM SPSS v23 (IBM Corporation, Armonk, New York, USA) was utilized considering HA and β-TCP ratios as independent variables, thus Ca:P ratio and Ca and PO_4 ion concentrations were considered as dependent variables.

3 Results

The ICP results were used to verify the Ca:P ratio of the two individual materials, in each of the 3 experimental states: (i) raw (as received), (ii) after calcination (800 ℃), and (iii) post sintering (1100 ℃) (Fig. 2(a)). The trend in the β-TCP group shows an initial decrease from raw state to after calcination state, but then an increase in post sintering state. The Ca:P ratio slightly increases while going from raw, to calcined, and ultimately sintered state in the HA group. The one-way ANOVA statistical analysis results in $p = 0.0204$ and $p = 0.022$, for HA and β-TCP respectively, indicating significant effect due to the state of the material. Energy-dispersive X-ray spectroscopy (EDS) was completed to evaluate the Ca/P ratio for experimental scaffolds of 100% HA, 100% β-TCP, and 15%/85% HA/β-TCP. The Ca/P ratios observed for the different groups are similar to what is expected aside from 100% HA, which seems to be slightly on the lower end of the atomic value of ~1.67 (Fig. 2(b)). The EDS was done as a supplemental quantitative verification measurement on the primary sample groups. These values are taken as an estimate of final average of the groups.

XRD spectra were collected of the individual raw materials for crystalline verification. Their spectra were matched to the theoretical HA and β-TCP. After confirmation of the materials was complete, and the experimental colloidal gels were fabricated and subjected to sintering at 1100 ℃, XRD spectra were obtained from the groups for crystalline phase determination and verification (Fig. 3(a)). The β-TCP phase is indicated by three high intensity peaks located

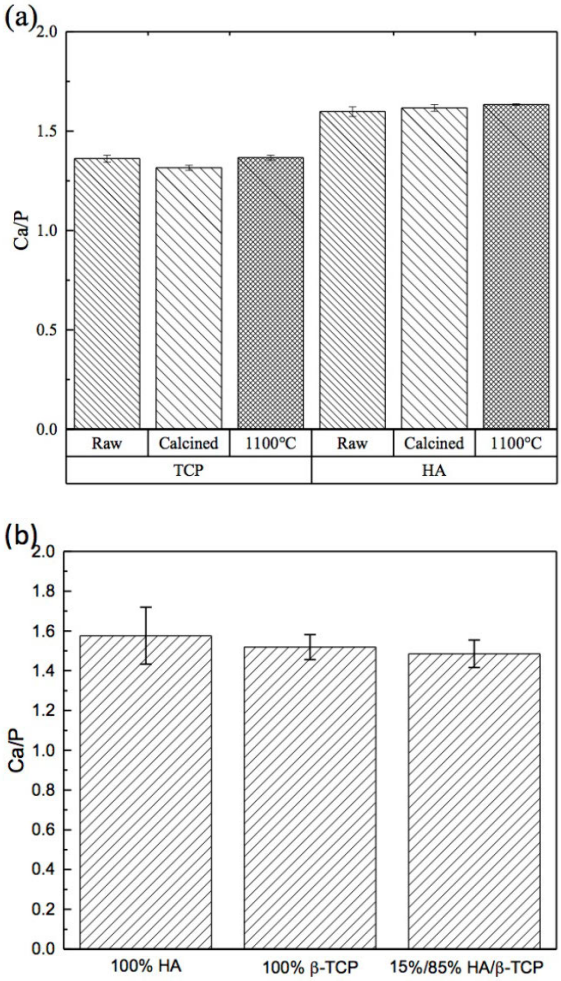

Fig. 2 (a) Mean ± 95% confidence intervals for Ca/P ratio depicting the two primary groups (HA and β-TCP) and their state. (b) Mean ± 95% confidence intervals for Ca/P ratio of the experimental groups.

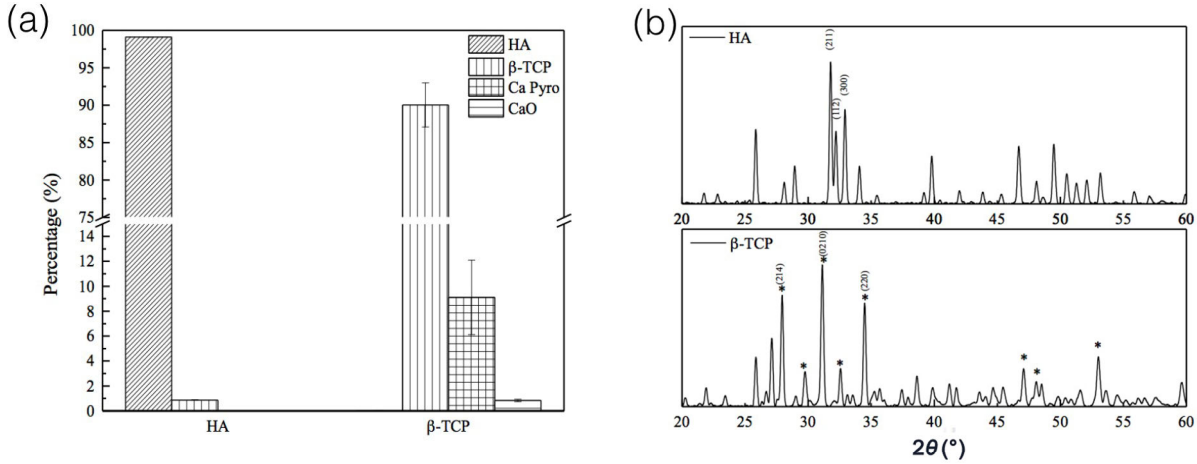

Fig. 3 (a) Percentage of each phase of the as-received raw materials prior to calcination (β-TCP vertical filled bars, calcium pyrophosphate (Ca Pyro) in hatched bars, and calcium oxide represented in horizontal filled bars). (b) The XRD spectra are a comparison between the two basic components of the ink. The upper box represents the XRD spectrum of hydroxyapatite (HA) group while the lower box represents the β-TCP group. A few of the most intense diffraction peaks are shown.

at 27.9°, 31.2°, and 34.4°, while the highest peaks for HA are 31.8° and 32.9° (Fig. 3(b)). High crystallinity is indicated by the narrow diffraction peaks described as sharp peaks. This result is in good agreement with other researchers' works that found that biphasic mixing on a crystallite level is feasible [16–18].

The calcium (Ca) and phosphate (PO_4) concentrations (mg/dL) of scaffold dissolution in Tris-HCl solution are summarized in Table 2. Figure 4 indicates that the data, which begin at time point of 0 h to indicate the initial, are used for analysis of both calcium and phosphate. The 100% HA scaffold group shows the greatest concentration of Ca ions (~1.9 mg/dL), but ultimately releases at a lower amount, which can be seen at hour 336 (day 14). The 100% HA scaffold has the lowest amount of calcium ions released. On the other end of the materials, the 100% β-TCP has the highest concentration released with approximately a measurement of 7.6 mg/dL. The 15%/85% HA/β-TCP scaffold group falls in between the 100% HA and 100% β-TCP groups, and at day 14 has a Ca ion release of approximately 5.95 mg/dL.

While the PO_4 ion release shows a similar trend as that in Ca with one apparent difference in the 100% HA scaffold group. There is nearly 0 mg/dL of the phosphate ion released in the first 24 h, in comparison to the amount of Ca ions released during the same time frame. The 100% HA group eventually ends up having a release of approximately 5.1 mg/dL at day 14, but it is short of what the other three groups (100% β-TCP, 15%/85% HA/β-TCP, and 15%/85% HA/β-TCP (design)) release in the same time period. 100% β-TCP,

Table 2 Ca and PO_4 mean concentration as released from the mono- and bi-phasic scaffold groups; the standard deviations are noted in parentheses (Unit: mg/dL)

Group		Element	Time (h)							
			1	12	24	72	168	216	288	336
Monophasic	HA	Ca^{2+}	1.864 (0.13)	1.971 (0.24)	2.015 (0.04)	3.874 (0.05)	2.463 (0.62)	3.659 (0.48)	4.540 (0.31)	4.469 (0.04)
		$(PO_4)^{3-}$	0.079 (0.06)	0.089 (0.09)	0.108 (0.05)	0.952 (0.00)	2.112 (0.17)	2.284 (0.04)	3.882 (0.75)	5.112 (0.59)
	β-TCP	Ca^{2+}	1.485 (0.08)	2.015 (0.31)	2.256 (0.28)	5.250 (0.76)	5.675 (0.15)	6.129 (0.31)	7.349 (0.23)	7.632 (0.65)
		$(PO_4)^{3-}$	1.304 (0.18)	1.636 (0.14)	1.939 (0.03)	4.265 (0.44)	7.183 (0.19)	7.525 (1.59)	7.912 (0.34)	7.912 (1.01)
Biphasic	HA/β-TCP	Ca^{2+}	1.044 (0.03)	1.318 (0.08)	1.606 (0.13)	3.601 (0.38)	4.245 (0.03)	4.621 (0.62)	5.510 (0.16)	5.947 (0.16)
		$(PO_4)^{3-}$	1.099 (0.13)	1.788 (0.23)	2.367 (0.36)	4.659 (1.29)	6.685 (0.48)	8.097 (0.06)	8.496 (0.91)	8.581 (0.34)
	HA/β-TCP (design)	Ca^{2+}	0.770 (0.03)	0.914 (0.04)	1.215 (0.01)	2.555 (0.03)	3.465 (0.14)	3.426 (0.26)	4.038 (0.27)	4.437 (0.16)
		$(PO_4)^{3-}$	1.056 (0.05)	1.830 (0.08)	2.468 (0.26)	4.752 (0.48)	7.373 (0.57)	8.097 (0.59)	8.221 (0.72)	9.346 (0.92)

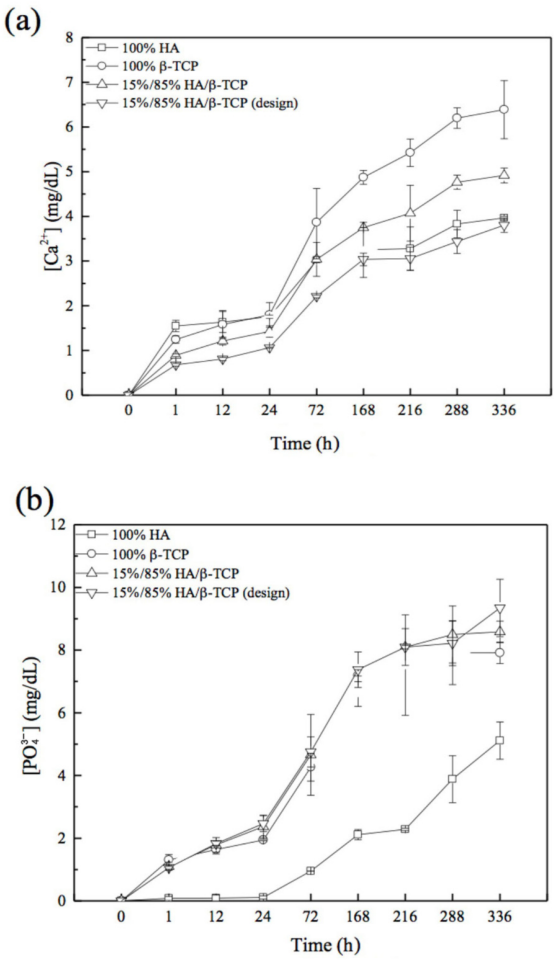

Fig. 4 (a) Ca concentration and (b) PO_4 concentration in 0.05 mol/L Tris buffer after immersion of 100% HA, 100% β-TCP, 15%/85% HA/β-TCP, and 15%/85% HA/β-TCP (design) for time periods ranging from 1 to 336 h (14 days).

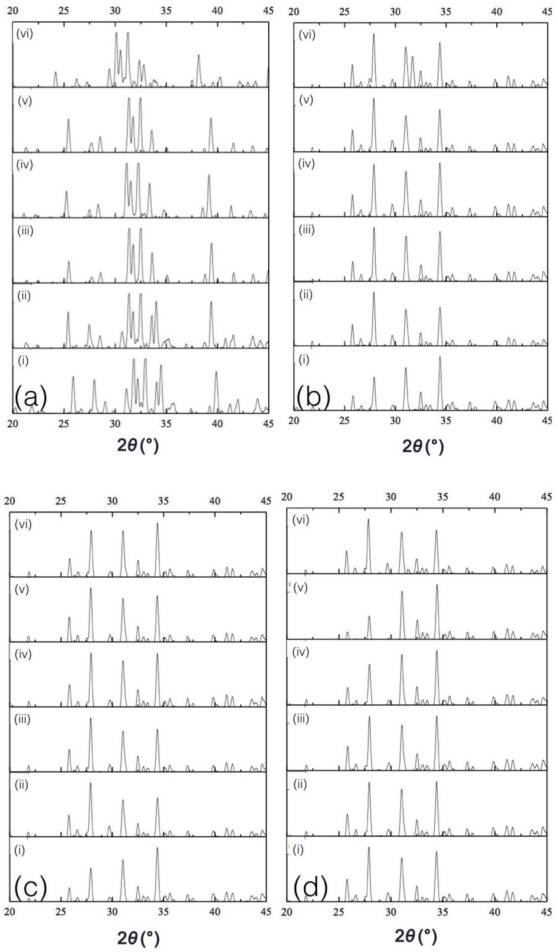

Fig. 5 These XRD spectra are for groups (a) 100% HA, (b) 100% β-TCP, (c) 15%/85% HA/β-TCP, and (d) 15%/85% HA/β-TCP (design) and are a comparison among the six time points *in vitro*: (i) initial, (ii) 1 day, (iii) 7 days, (iv) 14 days, (v) 21 days, and (vi) 28 days.

15%/85% HA/β-TCP, and 15%/85% HA/β-TCP (design) follow the same trend, and at day 14, they all have an average PO_4 ion concentration of ~8.61 mg/dL, with no significant difference between these three experimental scaffolds' compositions. Additionally, the experimental scaffolds' compositions were analyzed after the time *in vitro*, to verify no changes in phases. As seen in Figs. 5(a)–5(d), when evaluating the relevant peaks, no differences are observed from time 0 thru 28 days, indicating that the material remains unaffected over time.

4 Discussion and conclusions

Being that a wide range of physical and chemical properties can be achieved with this particular bioactive ceramic by modifying specific parameters, such as the HA/β-TCP ratio, calcining and/or sintering temperature [19], these materials have been used to fabricate pre-formed implants and have shown considerably greater mechanical strength in comparison to other bioceramics used for similar bone grafting purposes [19]. The present study aimed to chemically characterize bioactive ceramic LBBCS prepared as 100% HA, 100% β-TCP, 15%/85% HA/β-TCP, and a model 15%/85% HA/β-TCP group with raw materials calcined at 800 ℃, and final LBBCS subjected to a sintering regimen of 1100 ℃.

The advantage of this material, which is fabricated to an aqueous paste, allows for fabrication of scaffolds utilizing solid free form (SFF) equipment also known as robocasting. This 3D printing technique allows for the production of variety of complex structures utilizing CAD/CAM software in addition to utilizing computed

tomography scans exported to a specific file type which can in turn be fabricated to a specific defect, capable of reproducing the same structure consistently [20].

XRD of the as-received materials prior to calcination primarily showed HA and β-TCP crystalline phases for the individual HA and β-TCP powders. However, phase quantification through Rietveld refinement showed trivial fractions of β-TCP, calcium pyrophosphate ($Ca_2P_2O_7$), and calcium oxide (CaO) for the HA as-received material, and minor fractions of HA, $Ca_2P_2O_7$, and CaO for the β-TCP starting material. Given that the aqueous pastes were fabricated without considering the presence of minor quantities of other CaP-based phases, the intended composition of the 15%/85% HA/β-TCP group was slightly shifted from what was originally intended.

Phosphorus (P) is widely distributed in the body. More than 80% of total phosphate (PO_4) is present in the bone and teeth in the form of apatite. The remaining phosphate is mostly present in the skeletal muscle, with trace amounts in the extracellular fluids (< 0.1%) [21–24]. Intracellular phosphate ions are essential for oxidative phosphorylation and approximately 20% of cellular phosphate is present in the mitochondria. Roughly 30% of total cellular phosphate is stored in the endoplasmic reticulum and is used in phosphorylation of various proteins. The remaining cellular phosphate is present in the nucleus, Golgi complex, and lysosomes. Transporting phosphate in and out of the cell according to the need of the body is a complex process and the exact molecular mechanisms of such sensitive transport are not entirely clear. It is important to note that cells use PO_4 to transport cellular energy through the formation of ATP by oxidative phosphorylation.

With the aforementioned, phosphorus is an essential nutrient for the body and is routinely consumed through food. After consumption, phosphorus binds with oxygen and exists as PO_4 in the body. Both organic and inorganic forms of PO_4 are present in regularly consumed foods. The amount of total PO_4 ingestion can be significantly influenced by consumption of processed food and beverage, as there are phosphate metabolites additives in these items. Following a meal, inorganic phosphate can be rapidly absorbed across the small intestine and enter the blood stream causing an elevation in blood phosphate levels. The net efficiency of intestinal phosphate absorption is double that of Ca [25]. Taking into consideration just the amount of phosphate consumed and adding a calcium phosphate (CaP)-based scaffold can lead to a potential toxic situation. Phosphate toxicity due to excessive retention of PO_4 in the body can cause a variety of cellular and tissue damage. An example is seen with the higher occurrence of vascular calcification, encountered in patients with chronic kidney disease, is related to the increased retention of phosphate in the body [26,27]. The normal range of PO_4 should be in the order of 2.4–4.1 mg/dL, so this is of importance as when scaffold is placed in the system, the levels in the local region may be slightly higher than normal, but should not increase the overall levels to prevent any complications such as cell death, which in turn would lead to killing new bone cells.

Chen *et al.* [28] and Sweet *et al.* [29] have studied the *in vitro* analysis of ion release in the SBF solution, with regards to cytotoxicity. The cytotoxicity assay results indicated that the 100% β-TCP material, which is most commonly used, did not have a negative effect on altering the Schwann cells *in vitro*.

The data from the *in vitro* portion of this study is in agreement with literature. Using the 100% HA and 100% β-TCP as controls and the two 15%/85% HA/β-TCP groups as the experimental groups, the results are similar to what was expected. Literature presents the bulk or pressed powder properties of these two control group materials, but does not present the biphasic mixture release for Ca or PO_4 in an *in vitro* setting. The results indicate the trend for the two biphasic groups, in which the rates of calcium and phosphate ion release should fall above the 100% HA but below 100% β-TCP. This was the result, which was observed when doing a qualitative analysis of the results and further identified with the extrapolation of data from previous bulk property results.

Overall, since various chemical formulations can lead to different physiochemical properties of these extruded materials processed, it is important to understand how the tailoring of this important biphasic material can impact the long-term outcome of an ever-important *in vivo* clinical trial in the future.

As the scaffolds can be fabricated from mixing various ratios of the bioactive ceramic, HA and β-TCP, both of which are biocompatible, resorbable, and can facilitate in the regeneration and remodeling of bone at defect site, the results are important on how to tailor composition. Custom ratios of the materials in scaffolds for use in load and non-load bearing models are warranted to explore the rate of osseointegration, as the release of these ions has the potential to dictate which material would be of use in the final scaffold design.

References

[1] LeGeros RZ, Parsons JR, Daculsi G, *et al*. Significance of the porosity and physical chemistry of calcium phosphate ceramics biodegradation–bioresorption. *Ann NY Acad Sci* 1988, **523**: 268–271.

[2] Daculsi G, LeGeros RZ, Nery E, *et al*. Transformation of biphasic calcium phosphate ceramics *in vivo*: Ultrastructural and physicochemical characterization. *J Biomed Mater Res* 1989, **23**: 883–894.

[3] Heughebaert M, LeGeros RZ, Gineste M, *et al*. Physicochemical characterization of deposits associated with HA ceramics implanted in nonosseous sites. *J Biomed Mater Res* 1988, **22**: 257–268.

[4] Ducheyne P, Radin S, King L. The effect of calcium phosphate ceramic composition and structure on *in vitro* behavior. I. Dissolution. *J Biomed Mater Res* 1993, **27**: 25–34.

[5] Duheyne P, Beight J, Cuckler J, *et al*. Effect of calcium phosphate coating characteristics on early post-operative bone tissue ingrowth. *Biomaterials* 1990, **11**: 531–540.

[6] Ducheyne P, Cuckler JM. Bioactive ceramic prosthetic coatings. *Clin Orthop Relat R* 1992, **76**: 102–114.

[7] Witek L, Smay J, Silva NRFA, *et al*. Sintering effects on the chemical and physical properties of bioactive ceramic rods biomaterials and biomimetics. New York University, 2011.

[8] Radin SR, Ducheyne P. Plasma spraying induced changes of calcium phosphate ceramic characteristics and the effect on *in vitro* stability. *J Mater Sci: Mater Med* 1992, **3**: 33–42.

[9] De Groot K, Klein C, Wolke JGC, *et al*. Plasma-sprayed coatings of calcium phosphate. *CRC Handbook of Bioactive Ceramics* 1990, **2**: 133–142.

[10] Vasiliu CEC. Assembly of hydroxy apatite: β tricalcium phosphate: Calcium sulfate bone engineering scaffolds. Master Thesis. Oklahoma State University, 2008.

[11] Szpalski C, Nguyen PD, Vasiliu CEC, *et al*. Bony engineering using time-release porous scaffolds to provide sustained growth factor delivery. *J Craniofac Surg* 2012, **23**: 638–644.

[12] Simon JL, Michna S, Lewis JA, *et al*. *In vivo* bone response to 3D periodic hydroxyapatite scaffolds assembled by direct ink writing. *J Biomed Mater Res* 2007, **83A**: 747–758.

[13] Mijares DQ. Synthetic bone mineral (SBM): Prevention of bone loss induced by estrogen deficiency in a rat model. New York: NYU College of Dentistry, 2009.

[14] Taylor JC, Hinczak I. Rietveld made easy: A practical guide to the understanding of the method and successful phase quantifications. Sietronics Pty Limited, 2006. Available at http://www.ccp14.ac.uk/ccp/web-mirrors/commercial/siroquant/siroqnt/pdfs/rmeintro.pdf.

[15] Rietveld HM. *The Rietveld Method*. Oxford University Press, 1993.

[16] Nilen RWN, Richter PW. The thermal stability of hydroxyapatite in biphasic calcium phosphate ceramics. *J Mater Sci: Mater Med* 2008, **19**: 1693–1702.

[17] Daculsi G. Biphasic calcium phosphate concept applied to artificial bone, implant coating and injectable bone substitute. *Biomaterials* 1998, **19**: 1473–1478.

[18] Amera A, Abudalazez AMA, Ismail RA, *et al*. Synthesis and characterization of porous biphasic calcium phosphate scaffold from different porogens for possible bone tissue engineering applications. *Sci Sinter* 2011, **43**: 183–192.

[19] Moore WR, Graves SE, Bain GI. Synthetic bone graft substitutes. *ANZ J Surg* 2001, **71**: 354–361.

[20] Miranda P, Saiz E, Gryn K, *et al*. Sintering and robocasting of β-tricalcium phosphate scaffolds for orthopaedic applications. *Acta Biomater* 2006, **2**: 457–466.

[21] Gaasbeek A, Meinders AE. Hypophosphatemia: An update on its etiology and treatment. *Am J Med* 2005, **118**: 1094–1101.

[22] Razzaque MS. The FGF23–Klotho axis: Endocrine regulation of phosphate homeostasis. *Nat Rev Endocrinol* 2009, **5**: 611–619.

[23] Iotti S, Lodi R, Gottardi G, *et al*. Inorganic phosphate is transported into mitochondria in the absence of ATP biosynthesis: An *in vivo* ^{31}P NMR study in the human skeletal muscle. *Biochem Bioph Res Co* 1996, **225**: 191–194.

[24] Hutson SM, Williams GD, Berkich DA, *et al*. A phosphorus-31 NMR study of mitochondrial inorganic phosphate visibility: Effects of calcium(2+) and manganese(2+) and the pH gradient. *Biochemistry* 1992, **31**: 1322–1330.

[25] Razzaque M. Phosphate toxicity: New insights into an old problem. *Clin Sci* 2011, **120**: 91–97.

[26] Fukagawa M, Hamada Y, Nakanishi S, *et al*. The kidney and bone metabolism: Nephrologists' point of view. *J Bone Miner Metab* 2006, **24**: 434–438.

[27] Razzaque MS. Therapeutic potential of klotho-FGF23 fusion polypeptides: WO2009095372. *Expert Opin Ther Pat* 2010, **20**: 981–985.

[28] Chen J, Xu L, Chen S, *et al*. Transcriptional regulation of platelet-derived growth factor-B chain by thrombin in endothelial cells: Involvement of Egr-1 and CREB-binding protein. *Mol Cell Biochem* 2012, **366**: 81–87.

[29] Sweet L, Kang Y, Czisch C, *et al*. Geometrical versus random β-TCP scaffolds: Exploring the effects on Sschwann cell growth and behavior. *PLoS ONE* 2015, **10**: e0139820.

Open Access The articles published in this journal are distributed under the terms of the Creative Commons Attribution 4.0 International License (http://creativecommons.org/licenses/by/4.0/), which permits unrestricted use, distribution, and reproduction in any medium, provided you give appropriate credit to the original author(s) and the source, provide a link to the Creative Commons license, and indicate if changes were made.